Friction **4**(3): 249–256 (2016)
DOI 10.1007/s40544-016-0122-x
ISSN 2223-7690
CN 10-1237/TH
RESEARCH ARTICLE

Morphology-influenced wetting model of nanopore structures

Sunghan KIM[†], Hyunho CHOI, Andreas A. POLYCARPOU, Hong LIANG[*]

Department of Mechanical Engineering, Texas A&M University, College Station, Texas 77843-3123, USA

[†] Present Address: School of Materials Science and Engineering, Georgia Institute of Technology, Atlanta 30332, USA

Received: 06 March 2016 / Revised: 07 June 2016 / Accepted: 14 July 2016

Abstract: Understanding the wetting behavior of nanostructures is important for surface design. The present study examined the intrinsic wettability of nanopore structures, and proposed a theoretical wetting model. Using this model, it was found that the wetting behavior of nanopore structures depends on the morphology of a surface. To accurately predict the wetting behavior of nanopore structures, correction factors were introduced. As a result, the proposed wetting model can be used to predict the wettability of nanopore structures for various engineering purposes.

Keywords: nanopore structures; wetting model; wettability; contact angle

1 Introduction

Understanding the wetting characteristics of surfaces is important for microfluidics, self-cleaning, anti-icing, bio-sensing, and filtration processes [1–11]. It is known that a substrate with low surface energy will have a large contact angle with deionized water, while high surface energy on any given substrate will produce a small contact angle [12]. This signifies that the contact angle can represent a substrate's surface energy. One example can be found in Fujii et al. that report that nanostructures of a surface influence wettability [13]. There are three models to explain the relationship between surface energy and contact angle, as follows: Young's model, Cassie-Baxter model, and Wenzel's model. Young's wetting model explains the wettability of a perfectly smooth, flat surface when a liquid droplet is placed on the surface [14]. Most surfaces are not atomically smooth, and surface roughness is a crucial factor in explaining a surface's wetting characteristics. Two models that have been widely used to predict wetting characteristics for rough surfaces are the Cassie-Baxter model and the Wenzel's model [15, 16]. The Cassie-Baxter model is suited to clarify the wetting state of heterogeneous surfaces where air pockets are present between the liquid droplet and the surface. Wenzel's model can be used to determine the wetting state of homogeneous surfaces where full contact occurs between a liquid and solid, with no air pockets.

In both the Cassie-Baxter and Wenzel's models, the contact angle is determined by the fraction of the solid surface area that is in contact with the liquid, that is, the fraction that is wet. As such, the contact angle is affected by the surface morphology. Kim et al. proposed a modified Cassie-Baxter equation in order to predict contact angle values on microline patterned surfaces [17]. Han et al. performed a quantitative analysis of the effect of pore size distribution on the wetting behavior of nanostructured surfaces, proposing a modified version of Wenzel's model [18]. Notably, many studies have examined the wetting behavior of highly-ordered nanopore structures using specifically proposed wetting models [19–24]. As we have shown in our previous study, the trapped air in the pores is a critical parameter to determine the wetting behavior of nanopore structures [22]. Applying the theory of minimum interfacial free energy and force balance mechanism, Yang et al. developed a wetting model to

* Corresponding author: Hong LIANG.
E-mail: hliang@tamu.edu

investigate the contact angle of a droplet on alumina-based nanopore structures [23]. The relationship between contact angle and surface morphology can be used as a critical design parameter for surface wettability. These classic wetting models, however, are not suited for predicting the practical wetting behavior of water droplets on micro/nanostructured surfaces [25, 26].

Defining the exact localized area of solid–liquid and liquid–air interfacial sections near the triple-phase contact line (TCL) is critical to understand the wetting behavior. To verify the localized area at TCL, a detailed analysis of surface morphology is needed. Luo et al. developed geometrical models of surface profiles that could predict the contact angle of microscale laser patterned surfaces [27]. Ran et al. reported that the wettability of nanoporous surfaces could be manipulated by the shape of a hole [19]. Previous studies on patterned structures, however, have not sufficiently considered the form of nanoscale surface structures. The present study established a new surface shape-dependent wetting model of nanopore patterned structures by employing correction factors. Correction factors were determined for both shape and volume to verify the wettability of nanopore structures. The proposed model has been used to perform a numerical simulation to calculate the contact angle values. These values have been verified by experiments. Results showed that when correction factors were introduced, the proposed wetting model was able to effectively predict the wetting behavior of nanopore structures.

2 Experimental details

2.1 Preparation of nanopore structures

Nickel based metallic nanopore structures were prepared for the wetting experiments. The metallic nanopore structures are composed of nickel [28] and had various pore sizes in the range of 150 to 380 nm. The alumina nanopore structures were used as a template to fabricate the metallic nanopore structures. A pure aluminum foil (99.999%, thickness: 1 mm) was used as a base material to fabricate the alumina nanopore structures. Electropolishing was performed with a mixture of ethanol and perchloric acid (C_2H_5OH: $HClO_4$ = 4:1 by volumetric ratio) to get rid of surface irregularities and the oxide film. The temperature was maintained at 7 ℃ and a 20 V DC electrical potential was applied during the electro-polishing process. By using deionized water and ethanol, the electropolished aluminum was rinsed. To perform a first anodization process, after rinsing, the electropolished aluminum was treated with applying 195 V DC in 0.1 M phosphoric acid for 8 hours at 0 ℃. During the first anodization process, randomly formed nanopore structures, which have uniformly dimpled aluminum substrate at the bottom, were created on the top surface. After the first anodization, the randomly formed alumina nanopore structure was etched with a mixed solution of chromic acid (1.8 wt%) and phosphoric acid (6 wt%) for 5 hours at 65 ℃. The etched substrate was rinsed with deionized water and ethanol.

A second anodization process was performed with the same anodizing conditions used in the first anodization process for 10 minutes. Orderly arrayed alumina nanopore structures were fabricated by the second anodization process. The initial diameter of the pores was about 100 nm, the inter-pore distance was about 500 nm, and the total thickness was about 1 μm. The diameter of pores can be widened through widening process with phosphoric acid (0.1 M) at 30 ℃. The pore widening rate was about 0.6 nm/min. A metal source (nickel) was deposited on top of the alumina nanopore structures by using an electron beam evaporator with 4 Å/s deposition rate in a vacuum of 5×10^{-6} Torr. Various pore size metallic nanopore structures were fabricated on the top surface of the alumina nanopore structures having different pore diameters: 154 ± 11 nm, 258 ± 14 nm, and 379 ± 18 nm. In order to fabricate a flat nickel substrate, the nickel was deposited on the top surface of polished silicon wafer.

2.2 Wetting experiments on nanopore stuructres

The metallic nanopore structures were used for the wetting/electrowetting experiments. The contact angle between water droplet and metallic nanopore structures with various pore sizes was evaluated using a digital camera (PowerShot SD750, Canon) combined droplet shape measurement system. A single water droplet of 2 μL deionized water was dropped on the substrates by a calibrated micropipette (VWR International).

Contact angle measurements were done by repeating 10 times.

3 Theoretical approach: Analysis of wettability on metallic nanopore structures

Using the principle of energy conservation, it is possible to solve the wettability of heterogeneous surfaces [29]. Based on both the energy balance concept and Young's equation, the wetting model for metallic nanopore structures can be defined with geometrical factors of a liquid droplet on metallic nanopore structures. To establish a basic wetting model for metallic nanopore structures, the surface net energy of a flat surface (a nonporous surface with no texture) should be considered. In order to understand the wetting behavior on the nanopore structures, the detailed shape of the pore should be considered in terms of correction factors. This will be discussed later. By combining the surface net energy on both the flat surface and the metallic nanopore structure, the following final equilibrium equation can be obtained [17, 23, 30]:

$$\cos\theta^* = \frac{(S_1^* + f_{\text{l-s}})\cos\theta + S_2 - S_2^* - f_{\text{l-v}}}{S_1} \tag{1}$$

where θ^* is the apparent contact angle between a metallic nanopore structure and a liquid droplet, S_1 is the area of liquid–solid interface on a flat surface, S_1^* is the area of liquid–solid interface on a metallic nanopore structure, $f_{\text{l-s}}$ is the area of liquid–solid on a nanopore structure, θ is the intrinsic contact angle between a flat surface and liquid droplet, S_2 is the area of liquid–vapor interface on a flat surface, S_2^* is the area of liquid–vapor interface on a metallic nanopore structure, and $f_{\text{l-v}}$ is the area of liquid–vapor in a nanopore shape. These variables can be verified by using the geometry of a liquid droplet on a surface, as depicted in Fig. 1. All area terms are represented by the interfacial contact length as the one-dimensional geometry. S_1, S_1^*, S_2, and S_2^* can also be defined from Figs. 1(a) and 1(b):

$$S_1 = 2r\cos\left(\theta - \frac{\pi}{2}\right) \tag{2}$$

$$S_1^* = 2r^*\cos\left(\theta^* - \frac{\pi}{2}\right) \tag{3}$$

$$S_2 = 2r\theta \tag{4}$$

$$S_2^* = 2r^*\theta^* \tag{5}$$

where r is the liquid droplet radius on a flat nonporous surface, r^* is the radius of a liquid droplet on a metallic nanopore structure. It is possible to resolve $f_{\text{l-s}}$ and $f_{\text{l-v}}$ from Fig. 1(c):

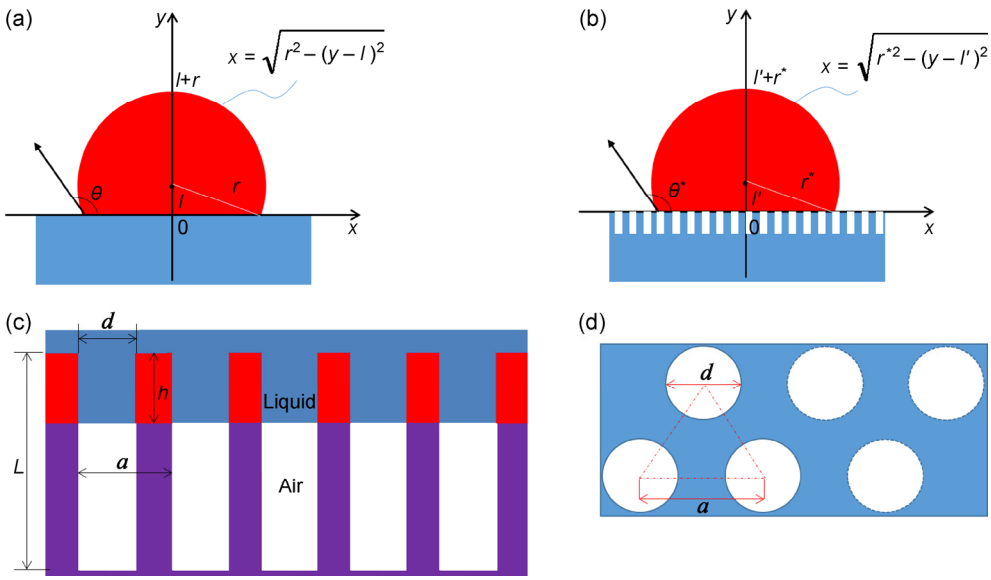

Fig. 1 Schematic diagrams of liquid droplet's geometries (a) on a flat nonporous surface, (b) on a metallic nanopore structure, (c) detail for the metallic nanopore structure, and (d) definition of the unit area of the metallic nanopore structure.

$$f_{\text{l-s}} = z\left(\frac{2h+a-d}{a}\right)2r^{*}\cos\left(\theta^{*}-\frac{\pi}{2}\right) \quad (6)$$

$$f_{\text{l-v}} = \left(\frac{d}{a}\right)2r^{*}\cos\left(\theta^{*}-\frac{\pi}{2}\right) \quad (7)$$

where z is the shape correction factor, a is the pore-to-pore distance (interpore distance), d is the pore diameter, and h is the absorption depth of a liquid droplet in the pore. The actual shape of metallic nanopore structures is of crown shape [31]. Due to the shape difference between the schematic model and the actual features, the shape correction factor "z" should be considered to calculate $f_{\text{l-s}}$.

Figure 2 shows the geometric difference between the actual shape and the schematic model of a metallic nanopore structure. The discrepancy in the total length of the outline between the crown shape and the triangle shape is not significant. To simplify, for the calculation of the shape correction factor, we assumed that the total length of the outline of the crown shape is the same as the length of the outline of the triangle shape. The shape correction factor "z" can be determined under the assumption that the length of the outline of the crown shape is the same as the length of the outline of the triangle shape by:

$$z = \frac{2(h-t)+\sqrt{(a-d)^2+4t^2}}{a-d+2h} \quad (8)$$

where t is the distance from the top to the bottom of the crown shape. The height value is the key parameter for determining the geometrical correction factors. The exact value of the height should be given/known to calculate each correction factor, but this value is not limited. As Fig. 2(a) shows, the height value of t is about 300 nm. The height value can be manipulated by the condition of the deposition process. In this study, the nickel was deposited on the top surface of all nanopore structures under identical conditions, and thus the height was fixed to 300 nm. Thus, we assumed that the value is fixed for all other pore size structures.

The air pockets between the water droplet and the nanopores are critical factors to determine the wettability of nanopore structures. The air pockets affect the depth of the absorbing water droplet on nanopore structures, and the air pockets operate to resist absorbing water into the pore [22, 32]. The absorption depth of the liquid droplet in the pore can be expressed under the assumption that the size of the single pore is much smaller than the size of the liquid droplet [19]:

$$h = \frac{4L\gamma\cos\theta}{P_0 d + 4\gamma\cos\theta} \quad (9)$$

where P_0 is the atmospheric pressure, γ is the surface tension of the surface, and L is the pore depth. In order to determine $f_{\text{l-v}}$, it is assumed that the liquid–air interface is flat. The variables of d, P_0, γ, L, θ, and a are all known values. Using Eqs. (2)–(9), it is possible to set Eq. (1) as a function of θ^{*}, r^{*}, and r. In order

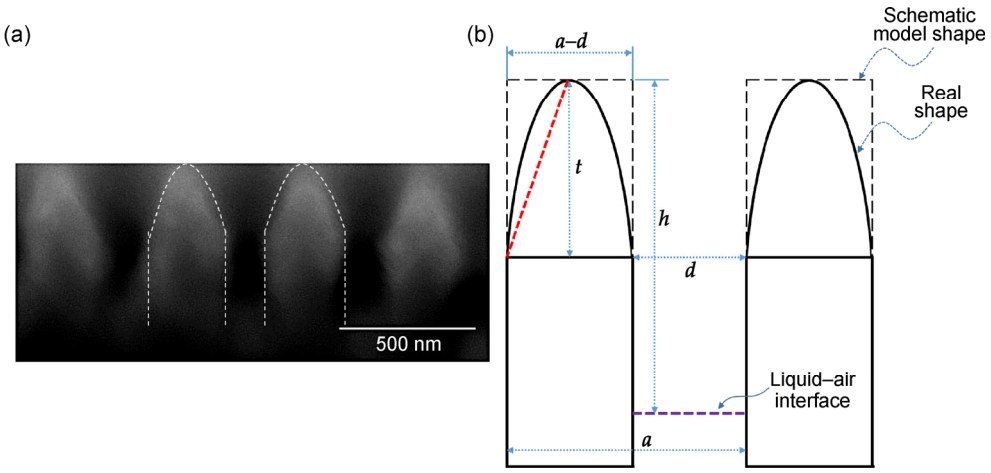

Fig. 2 SEM image and schematic diagram for calculating the area of the liquid–solid interface at the nanopore shape and the area of liquid–vapor interface in the nanopore shape. The SEM image in (a) shows a cross-section of a metallic nanopore structure, and (b) is a simplified cross-section geometry of a pore shape.

to determine θ^*, $r^*$and r should be verified with the volume conditions of liquid droplets. The volume conditions are determined from Figs. 1 and 2:

$$V_{\text{flat}} = \pi\left(-\frac{\left(r\sin\left(\theta-\frac{\pi}{2}\right)\right)^3}{3}+r^3\sin\left(\theta-\frac{\pi}{2}\right)+\frac{2r^3}{3}\right) \quad (10)$$

$$V_{\text{nanopore}} = \pi\left(-\frac{\left(r^*\sin\left(\theta^*-\frac{\pi}{2}\right)\right)^3}{3}+r^{*3}\sin\left(\theta^*-\frac{\pi}{2}\right)+\frac{2r^{*3}}{3}\right) + \alpha\left(\pi\left(\frac{d}{2}\right)^2 h\right)\frac{3}{\left(\frac{3\sqrt{3}}{2}a^2\right)}\pi\left(r^*\cos\left(\theta^*-\frac{\pi}{2}\right)\right)^2 \quad (11)$$

$$\alpha = \frac{a^2h+2d^2(h-t)}{3hd^2} \quad (12)$$

where V_{flat} is the volume of a liquid droplet on a flat nonporous surface, V_{nanopore} is the volume of a liquid droplet on a metallic nanopore structure, and α is the volume correction factor. The α is used to determine the volume difference between the schematic model and the crown shape of the actual shape. The volume correction factor "α" is defined as the ratio of the volume of a liquid droplet inside the actual (crown-shape) nanopore structure to the volume of a liquid droplet inside the simplified (schematic) nanopore strucutre. By using the volume correction factor "α", it is possible to compensate the volume difference between the actual shape and the simplified shape of nanopore structures. The volume of liquid droplets on both a flat nonporous surface and a metallic nanopore structure is the same, and thus has a constant value of $2\mu l$. Wettability behavior on a metallic nanopore structure can be verified by calculating θ^*, which can be numerically solved. All the parameters used in the model are shown in Table 1.

Table 1 Parameters used in the model for contact angle prediction of metallic nanopore structures.

P_0 (N/m^2)	a (nm)	L (nm)	θ (degree)	t (nm)	γ (N/m)	V (mm^3)
101300	500	1000	84.5	300	1.77	2.00

4 Results and discussion

Simulation and experimental results for different contact angles on the three different nanopore surfaces are shown in Fig. 3. A consistent trend of over-predicting the contact angles can be seen, as well as the fact that both model and experiment show an increasing trend (of contact angle) with pore diameter. The deviations between the results are nearly equal across all pore sizes. The first divergence is seen between the simulation results as calculated *without* and *with* correction factors. The contact angle values calculated using the proposed wetting model that accounted for correction factors (*z:* Eq. (8) and α: Eq. (12)) are closer to the actual experimental results, compared to the wetting model without correction factors (z=α=1). That is, the gaps between the results of the two different simulations point toward the importance of correction factors. The second divergence is between the simulation results as calculated with the inclusion of correction factors and the actual experimental results. Surface energy variation, a result of oxidation effects or surface irregularities, is likely the primary reason for the discrepancies between the simulation results and the experimental results [21, 23].

The results show that variations in surface energy affected the error occurrence in a linear manner. Concretely, the effect of surface irregularities on the simulation results can be verified by images of the nanopore structures' surfaces. Figure 4 shows

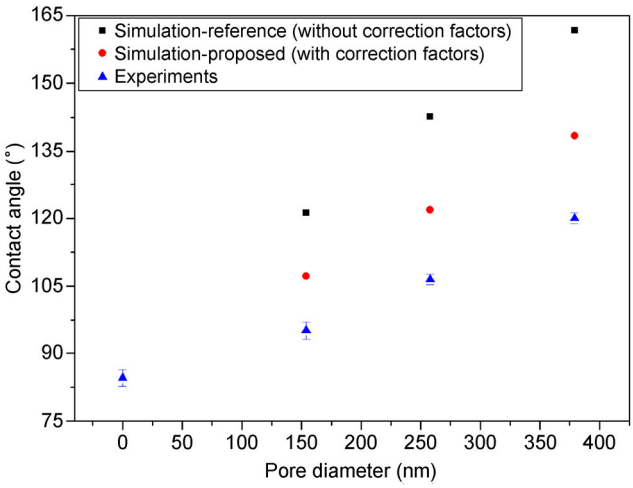

Fig. 3 Comparison of contact angle model predictions and experimental measurements of metallic nanopore structures versus pore size. Error bars show ± one standard deviation.

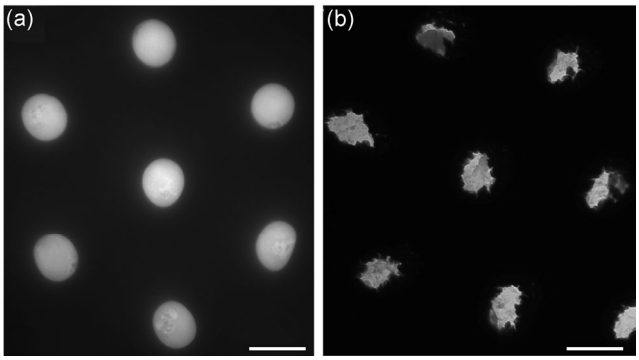

Fig. 4 TEM images of (a) alumina and (b) metallic nanopore structures. The scale bar represents 200 nm.

transmission electron microscopy (TEM) images of both alumina (a) and metallic (b) nanopore structures illustrating the different pore shapes. As the figure shows, the shape of each nanopore is different. The thickness of both samples, i.e., the metallic nanopore structures and the alumina nanopore structures, was about 500 nm. The pores of the alumina nanopore structures are clean, sharp, and nearly perfectly circular, whereas the pores of the metallic nanopore structures are irregular, uneven, and jagged. TEM images indicate that the molecules of nickel were irregularly deposited and progressively clogged the pore shape of the original substrate. It is difficult to control the uniformity of pore shape of nickel-based metallic nanopore structures during deposition. As such, the presence of surface irregularities is greater in the nickel-based metallic nanopore structures than in alumina nanopore structures. Such surface irregularities can increase the uncertainty of the simulation results.

Figure 5 shows the modeling and experimental results for the contact angles on alumina nanopore structures ($\gamma = 0.072$ N/m), based on data from the study published by Buijnsters et al. [21]. As the figure shows, the discrepancy between the simulation and experimental results is not significant. The reason is that, as mentioned earlier, the alumina nanopore structures have fewer surface irregularities, owing to their sharply defined pore shape. This result provides evidence that surface irregularities are the cause of the divergence between simulated and actual contact angle values. Thus, to compensate, surface irregularities can be used as an external parameter. This study argues that the proposed wetting model is well-suited to predicting the wettability of nanopore structures.

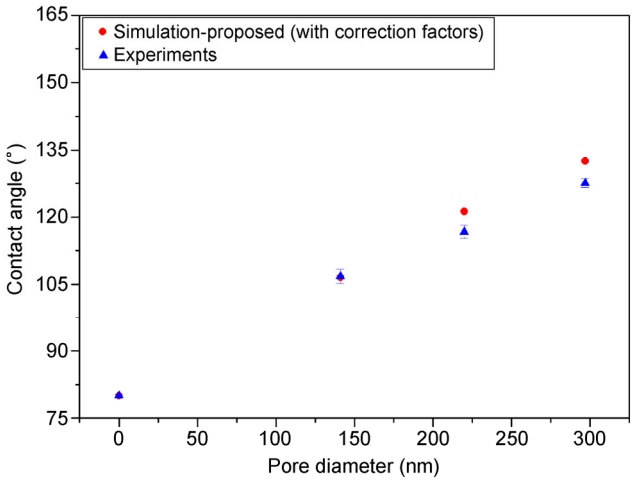

Fig. 5 Comparison of contact angle model predictions and experimental measurements of alumina nanopore structures (from Buijnsters et al. [21]) versus pore size. Error bars show ± one standard deviation.

5 Conclusions

In the present study, an improved wetting model was developed to simulate the intrinsic contact angle of highly ordered nanopore structures. Geometrical correction factors for shape and volume were introduced as critical elements for accurate calculation of contact angles. The experimentally measured contact angles were compared with the proposed wetting model results. The results showed that, when correction factors were applied, the wetting model worked well to simulate the wetting behavior of nanopore structures. Furthermore, to further improve the simulation results, an understanding of surface irregularities, in terms of surface energy variation, can be applied as an external parameter. The liquid–solid–air energy balance at the interface of water droplet, surface, and air pockets varies according to pore shape. This demonstrates that pore shape can be used to manipulate the contact phenomena that determine wettability. This study offers an improved wetting model for predicting the physical wetting behavior of nanopore structures, useful in designing surfaces for water treatment applications.

References

[1] Squires T M, Quake S R. Microfluidics: Fluid physics at the nanoliter scale. *Rev Mod Phys* **77**: 977–1026 (2005)

[2] Fürstner R, Barthlott W, Neinhuis C, Walzel P. Wetting and self-cleaning properties of artificial superhydrophobic surfaces. *Langmuir* **21**: 956–961 (2005)

[3] Rossi A M, Wang L, Reipa V, Murphy TE. Porous silicon biosensor for detection of viruses. *Biosens Bioelectron* **23**: 741–745 (2007)

[4] Bao S, Tang K, Kvithyld A, Engh T, Tangstad M. Wetting of pure aluminium on graphite, SiC and Al_2O_3 in aluminium filtration. *T Nonferr Metal Soc* **22**: 1930–1938 (2012)

[5] Cao L, Jones A K, Sikka V K, Wu J, Gao D. Anti-icing superhydrophobic coatings. *Langmuir* **25**: 12444–12448 (2009)

[6] Cao L, Price T P, Weiss M, Gao D. Super water-and oil-repellent surfaces on intrinsically hydrophilic and oleophilic porous silicon films. *Langmuir* **24**: 1640–1643 (2008)

[7] Haeberle S, Zengerle R. Microfluidic platforms for lab-on-a-chip applications. *Lab on a Chip* **7**: 1094–1110 (2007)

[8] Nguyen D D, Tai N-H, Lee S-B, Kuo W-S. Superhydrophobic and superoleophilic properties of graphene-based sponges fabricated using a facile dip coating method. *Energ Environ Sci* **5**: 7908–7912 (2012)

[9] Lai Y, Tang Y, Gong J, Gong D, Chi L, Lin C, Chen Z. Transparent superhydrophobic/superhydrophilic TiO_2-based coatings for self-cleaning and anti-fogging. *J Mater Chem* **22**: 7420–7426 (2012)

[10] Kim S, Zhou Y, Cirillo J D, Polycarpou A A, Liang H. Bacteria repelling on highly-ordered alumina-nanopore structures. *J Appl Phys* **117**: 155302 (2015)

[11] Choi H, Liang H. Wettability and spontaneous penetration of a water drop into hydrophobic pores. *J Colloid Interf Sci* **477**: 176−180 (2016)

[12] Blossey R. Self-cleaning surfaces–Virtual realities. *Nat Mater* **2**: 301–306 (2003)

[13] Fujii T, Sato H, Tsuji E, Aoki Y, Habazaki H. Important role of nanopore morphology in superoleophobic hierarchical surfaces. *J Phys Chem C* **116**: 23308–23314 (2012)

[14] Young T. An essay on the cohesion of fluids. *Philos T R Soc London* **95**: 65–87 (1805)

[15] Cassie A B D, Baxter S. Wettability of porous surfaces. *T Faraday Soc* **40**: 546–551 (1944)

[16] Wenzel R N. Surface roughness and contact angle. *J Phys Colloid Chem* **53**: 1466–1467 (1949)

[17] Kim D, Kim J, Hwang W. Prediction of contact angle on a microline patterned surface. *Surf Sci* **600**: L301–L304 (2006)

[18] Han T-Y, Shr J-F, Wu C-F, Hsieh C-T. A modified Wenzel model for hydrophobic behavior of nanostructured surfaces. *Thin Solid Film* **515**: 4666–4669 (2007)

[19] Ran C, Ding G, Liu W, Deng Y, Hou W. Wetting on nanoporous alumina surface: transition between Wenzel and Cassie states controlled by surface structure. *Langmuir* **24**: 9952–9955 (2008)

[20] Leese H, Bhurtun V, Lee K P, Mattia D. Wetting behaviour of hydrophilic and hydrophobic nanostructured porous anodic alumina. *Colloid Surf A: Physicochem Eng Aspects* **420**: 53–58 (2013)

[21] Buijnsters J G, Zhong R, Tsyntsaru N, Celis J-P. Surface wettability of macroporous anodized aluminum oxide. *ACS Appl Mater Interfaces* **5**: 3224–3233 (2013)

[22] Kim S, Polycarpou A A, Liang H. Electrical-potential induced surface wettability of porous metallic nanostructures. *Appl Surf Sci* **351**: 460–465 (2015)

[23] Yang J, Wang J, Wang C-W, He X, Li Y, Chen J-B, Zhou F. Intermediate wetting states on nanoporous structures of anodic aluminum oxide surfaces. *Thin Solid Film* **562**: 353–360 (2014)

[24] Raspal V, Awitor K, Massard C, Feschet-Chassot E, Bokalawela R, Johnson M. Nanoporous surface wetting behavior: The line tension influence. *Langmuir* **28**: 11064–11071 (2012)

[25] McHale G. Cassie and Wenzel: Were they really so wrong? *Langmuir* **23**: 8200–8205 (2007)

[26] Gao L, McCarthy T J. How Wenzel and Cassie were wrong. *Langmuir* **23**: 3762–3765 (2007)

[27] Luo B, Shum P W, Zhou Z, Li K. Surface geometrical model modification and contact angle prediction for the laser patterned steel surface. *Surf Coat Technol* **205**: 2597–2604 (2010)

[28] Kim S, Lee S, Choi D, Lee K, Park H, Hwang W. Fabrication of metal nanohoneycomb structures and their tribological behavior. *Adv Compos Mater* **17**: 101–110 (2008)

[29] Johnson Jr R E, Dettre R H. Contact angle hysteresis. III. Study of an idealized heterogeneous surface. *J Physl Chem* **68**: 1744–1750 (1964)

[30] Zu Y, Yan Y, Li J, Han Z. Wetting behaviours of a single droplet on biomimetic micro structured surfaces. *J Bionic Eng* **7**: 191–198 (2010)

[31] Choi D, Lee P, Hwang W, Lee K, Park H. Measurement of the pore sizes for anodic aluminum oxide (AAO). *Current Appl Phys* **6**: e125-e129 (2006)

[32] Li Z, Wang J, Zhang Y, Wang J, Jiang L, Song Y. Closed-air induced composite wetting on hydrophilic ordered nanoporous anodic alumina. *Appl Phys Lett* **97**: 233107 (2010)

Sunghan KIM. He is currently a postdoc at Georgia Institute of Technology. He graduated from Mechanical Engineering, Texas A&M University in 2015. His thesis research was focused on surface properties of porous structured materials.

Andreas POLYCARPOU. He is James J. Cain Chair and Meinhard H. Kotzebue'14 professor and department head of Mechanical Engineering at Texas A&M University. His tribological research has been primarily focused on contact mechanics related to miniature systems.

Hong LIANG. She is professor of Mechanical Engineering, Texas A&M University. Her research has been focused on fundamental understanding in surfaces and interfaces of various materials, in terms of their properties and tribological performance.